Materialia 7 (2019) 100418

Contents lists available at ScienceDirect

Materialia

journal homepage: www.elsevier.com/locate/mtla

Full Length Article

On the nucleation mechanism of {112} ⟨111⟩ mechanical twins in as-quenched β metastable Ti-12 wt.% Mo alloy

M. Marteleur[a,*], H. Idrissi[a,b], B. Amin-Ahmadi[c], F. Prima[d], D. Schryvers[b], P.J. Jacques[a]

[a] Institute of Mechanics, Materials and Civil Engineering (iMMC), IMAP, UCLouvain, Place Sainte Barbe 2, B-1348 Louvain-la-Neuve, Belgium
[b] EMAT, Department of Physics, University of Antwerp, Groenenborgerlaan 171, B-2020 Antwerp, Belgium
[c] Department of Mechanical Engineering, Colorado School of Mines, 1500 Illinois St, Golden, CO 80401, USA
[d] Chimie ParisTech - CNRS, Institut de Recherche de Chimie Paris, PSL Research University, 75005 Paris, France

ARTICLE INFO

Keywords:
Titanium alloys
Dislocations
Twinning
Work hardening
TEM

ABSTRACT

Recently developed β-metastable Ti grades take advantage of the simultaneous activation of TRIP and TWIP effects for enhancing their work hardening rate. However, the role of each plasticity mechanism on the macroscopic mechanical response is still unclear. In this work, the nucleation mechanism of the first activated plasticity mechanism, namely {112}⟨111⟩ twinning, was investigated. Firstly, post-mortem TEM analysis showed that twins nucleate on pre-existing microstructural defects such as thermal jogs with the zonal dislocation mechanism. The precipitation of the ω phase on twin boundaries has been observed, as well as the emission of numerous dislocations from super-jogs present in these twin boundaries. It is also shown that {112}⟨111⟩ twins act as effective dislocation sources for the subsequent plasticity mechanisms such as $\beta \rightarrow \alpha''$ martensitic transformation and {332}⟨113⟩ twinning. Secondly, *in situ* TEM tensile testing of the investigated Ti grade highlighted the primary role of the initial defect configuration present in the microstructure. It is shown that twins cannot nucleate without the presence of specific defects allowing the triggering of the dislocation decomposition needed for the twinning mechanism highlighted in investigated bulk samples.

1. Introduction

Among the various mechanisms of plastic deformation, mechanical twinning has gained more and more interest. Indeed, twinning has been observed in various crystallographic systems, regardless of the symmetry of the crystal lattice. Body-centered cubic (BCC) crystals can exhibit {112}<111> mechanical twinning, mostly when strained at low temperature. A faster increase of the flow stress for perfect dislocation glide than for twinning with decreasing temperature is often proposed as the explanation of this observation.

Twinning is also of primary importance in the global mechanical response. Indeed, twin boundaries (TB) can potentially play the role of barrier to dislocation glide resulting in pile-ups, as well as dislocation sources. Interactions between gliding dislocations and twins in BCC alloys have been theoretically discussed by Sleeswyk and Verbraak [1] and experimentally observed by Levasseur [2] in α-Fe and by Mahajan [3] in a Mo–Re alloy. Depending on the orientation of the Burgers vector with respect to the crossed twins, they concluded that the interactions could lead to growth or shrinkage of twins, while allowing complete transmission of the initial perfect dislocation.

Previous studies [4-6] showed that high levels of work hardening rate in specific metastable BCC β-Ti alloys can be reached owing to the simultaneous activation of several plastic deformation mechanisms, namely stress-induced martensitic (SIM) transformation and {332}<113> mechanical twinning. However, no complete understanding of these plasticity mechanisms, particularly of how their mutual interactions bring such an improvement of the work hardening has been proposed yet. Investigations of the very early stages of plasticity revealed also the activation of {112}<111> mechanical twinning [7]. Since this specific kind of mechanical twins has been often related to the initiation mechanisms of microcracks, for example in cold worked Fe–Si alloys [8], pure Mo [9-10] and pure Cr [11], a better analysis of the role of this plasticity mechanism is necessary to assess its implications in the deformation of metastable β-Ti alloys. Moreover, the activation of both {332}<113> and {112}<111> twinning systems within each grain was not expected. Indeed, it is generally admitted that only one twinning system is activated depending on several parameters such as the β phase stability [12] or the orientation of the parent grains with respect to the loading direction [13]. Hardly any result has been reported about the activation of both twinning systems.

* Corresponding author.
E-mail addresses: matthieu.marteleur@uclouvain.be (M. Marteleur), pascal.jacques@uclouvain.be (P.J. Jacques).

https://doi.org/10.1016/j.mtla.2019.100418
Received 3 April 2019; Accepted 28 July 2019
Available online 31 July 2019

The aim of the present study is to identify the formation mechanism as well as the role of {112}⟨111⟩ mechanical twins in the global mechanical behaviour of TRIP/TWIP titanium alloys. First, TEM foils of slightly plastically strained bulk samples have been characterised to identify the dislocations involved in the twinning process as well as their interactions with the freshly formed mechanical twins. Secondly, quantitative *in situ* TEM tensile testing of FIB-milled beams has been performed to understand the very first steps of twin nucleation. *In situ* mechanical twinning has recently been observed in low stacking fault energy (SFE) FCC metals like Au nanowires [14], but such direct observation of mechanical twinning in BCC alloys has hardly been reported in the literature.

2. Overview of mechanisms of {112}<111> twin formation

Different mechanisms of formation of {112}⟨111⟩ twin have been proposed in the literature without a complete consensus. Several detailed reviews dedicated to deformation twinning can be found in [15–17].

2.1. Dislocation-based mechanisms

The first model of BCC twinning was proposed by Cottrell and Bilby in 1951 [18]. It is based on the pole mechanism, where a sessile portion of a perfect $\frac{a}{2}[111]$ dislocation dissociates in a sessile $\frac{a}{3}[112]$ pure edge segment (the pole) and a glissile $\frac{a}{6}[11\bar{1}]$ partial twinning dislocation:

$$\frac{a}{2}[111] \rightarrow \frac{a}{6}[11\bar{1}] + \frac{a}{3}[112]$$

While the glissile part moves away from the pole on a (112) plane, thus leaving a stacking fault behind it, it cross-slips in order to curl around the pole dislocation, leading to an helicoidal shape. The twin thus grows from a monolayer fault nucleus. It is worth noting that the dissociation process is not energetically favourable.

Sleeswyk [19] adapted the Cottrell–Bilby model so that twinning nucleation results from more common dislocation configurations. Indeed, a three-layer twin nucleus is formed by the dissociation of a perfect $\frac{a}{2}\langle 111\rangle$ screw dislocation into three partials on three (112) planes with threefold symmetry according to the reaction:

$$\frac{a}{2}\langle 111\rangle \rightarrow \frac{a}{6}\langle 111\rangle + \frac{a}{6}\langle 111\rangle + \frac{a}{6}\langle 111\rangle$$

This dissociation reaction is energetically favourable. The author claimed that further twin growth arises by incorporation of crossing $\frac{a}{2}\langle 111\rangle$ screw dislocations by the pole mechanism of Cottrell and Bilby. However, this proposed dissociation reaction has been shown to be unstable [20], while one of the three partials has to cross-slip on another (112) plane for the global configuration to be a viable twin nucleus. Atomistic calculations performed by Vitek [20] suggested that the energy of creation of mono-layered stacking faults in the BCC lattice (both intrinsic and extrinsic, corresponding to the twinning and anti-twinning single layer faults) is too large. Vitek [20] concluded that multi-layered intrinsic stacking faults (I_n) on n successive {112} planes, with $n \geq 3$, could present sufficiently low energy to occur in practice, namely the twinning case.

Other authors (Crussard [21] and Cohen et al. [22]) suggested that dissociation of dislocations could arise on {110} planes instead of {112} planes. The corresponding dissociation reaction on the $(\bar{1}10)$ plane gives:

$$\frac{a}{2}\langle 111\rangle \rightarrow \frac{a}{8}\langle 110\rangle + \frac{a}{4}\langle 112\rangle + \frac{a}{8}\langle 110\rangle$$

However, calculation of the generalised stacking fault energy (γ) surfaces by Vitek [23] showed that no stable stacking fault could exist on {110} planes. Furthermore, experimental evidence of stacking faults in BCC materials has been scarcely reported so far. Stacking faults on {112} planes have been observed in tungsten specimens after heating by electrical discharge in the electron microscope, thus bringing consequent stresses in the foil and probably leading to the stabilisation of the stacking faults [24]. Stacking faults on {112} [25] and {310} [26] planes were also observed in annealed niobium. In both cases, segregation of impurities during annealing was argued as the source of decrease of stacking fault energy, allowing the observation of these stacking faults.

Another mechanism for nucleation of {112} twins was proposed by Priestner and Leslie [27]. They suggested that dissociation of dislocations is due to pile-ups on sessile jogs. These sessile jogs form at the intersections of slip planes by the reaction:

$$\frac{a}{2}[\bar{1}11] + \frac{a}{2}[1\bar{1}1] \rightarrow a[001]$$

The stress concentration induced by the pile-ups on the jogs brings about a chain reaction that produces the three $\frac{a}{6}[1\bar{1}1]$ twinning dislocations forming the twin embryo. The authors analysed the stress concentration required for different kinds of slip plane intersections and also gave some experimental evidence supporting their model in the case of α-Fe alloys.

More recently, Hsiung and Lassila [28] applied the mechanism depicted by Hirth [29] to explain their experimental results in the case of shock-induced deformation twinning in tantalum and tantalum alloys. This mechanism is an extension of the Cottrel–Bilby model based on the same dissociation reaction as Sleeswyk [19] on three successive and parallel {112} planes, but with the addition of a zonal dislocation with no net Burgers vector, a concept initially introduced by Kronberg for the HCP twinning case [30]. The dissociation reaction can be written as:

$$\frac{a}{2}\langle 111\rangle \rightarrow \textit{zonal dislocation}\begin{cases}\frac{-a}{6}\langle 111\rangle \\ \frac{a}{3}\langle 111\rangle + \textit{twinning dislocations}\end{cases}\begin{cases}\frac{a}{6}\langle 111\rangle \\ \frac{a}{6}\langle 111\rangle \\ \frac{a}{6}\langle 111\rangle\end{cases}$$

A particular dislocation structure with individual dislocation lines (jogs) two planes apart on {112} planes is mandatory in this mechanism. Hsiung and Lassila argued that the large number of jogs present in the characterised specimens explains its effectiveness. They claimed that these jogs can be either grown-in thermal jogs or generated by the interaction of dislocations activated during the onset of plasticity. They also showed that a different dissociation reaction could lead to the formation of platelets of ω phase instead of twins when the shock energy is sufficiently large since it requires the activation of $\frac{a}{3}\langle 111\rangle$ anti-twinning partial dislocation with much larger gliding energy than the one of $\frac{a}{6}\langle 111\rangle$ twinning dislocations. This mechanism was also successfully applied to mechanical twinning and ω transition in a Ti–23Nb–0.7Ta–2Zr–1.2O at.% alloy (also called Gum metal) deformed in compression [31].

Finally, Ojha et al. managed to model the {112} twin nucleation stress in Fe-based alloys with excellent agreement with experimental values [32]. They used the dissociation mechanism of Sleeswyk and calculated the generalised planar fault energy (GPFE) in order to introduce it in the general expression of the energy of the system.

Their calculations confirmed the suggestion of Vitek that the stable twin nuclei are made of three layers. According to them, the GPFE approach is effective in illustrating the importance of these parameters, which previously proposed models could not manage.

2.2. Shuffle mechanism

Wasilewski [33] proposed that a shuffle mechanism could lead to the formation of {112} twins. He argued that such a mechanism does not require a unique shear stress direction while it is also favoured by compressive straining, both facts commonly observed experimentally. He also suggested that the complete mechanism could be a mixture of shear and shuffle to reach the final twin configuration. In their generalised theory of deformation twinning, Bilby and Crocker [34] predicted all possible twinning modes for all crystal types by considering combinations of shear and shuffle. To the best of the author's knowledge, no experimental evidence supporting this shuffle mechanism has been reported yet.

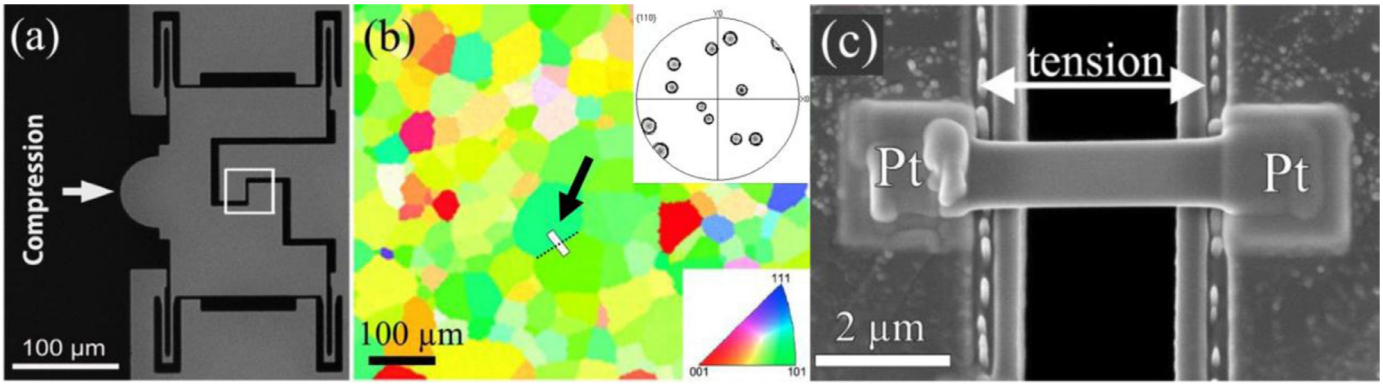

Fig. 1. (a) SEM micrograph of the push-to-pull MEMS device; (b) IPF map of the as-quenched Ti-12 wt.% Mo grade. The white line segment represents the location where the FIB-milled sample has been extracted and the dashed line is a grain boundary. Inset gives the stereographic projection of {110} poles of the two grains in the FIB-milled sample; (c) fixation of the sample on the PTP device.

In a recent study, Wu et al. [35] proposed a shuffle-based twinning model based on the β to ω phase transformation in a BCC Ti–30Nb–3Pd (wt.%) alloy. They suggested that the reverse transformation, from hexagonal to cubic phase, is the driving force for {112} twinning following the sequence:

$$\beta \rightarrow \omega \rightarrow \beta^{T}$$

The β to ω phase transformation arises by the collapse of two {111} planes [36]. In their model, Wu et al. [35] suggested that this mechanism occurs twice to form a twin embryo. They argued that the stability of the ω phase is the key parameter for {112} twinning since they did not observe twins in a Ti–30Nb (wt.%) grade where ω phase is more stable. Contradictorily, Lai et al. [37] demonstrated that the ω phase precipitation on twin boundaries in β-Ti alloys is a consequence of mechanical twinning, as a relaxation mechanism of the elastic strain appeared at the twin/matrix interface.

3. Experimental procedure

The investigated grade is the binary Ti-12 wt.% Mo alloy in which mechanical twinning has been previously reported [7]. Ingots were processed by arc melting from high-purity raw materials in Ar atmosphere. Several remelting cycles were performed to ensure chemical homogeneity of the ingots. The alloy was then heated to 1223 K for 15 min in air and water quenched to keep 100% β+ω_{ath} phase at room temperature. The ingots were cold rolled to a thickness of about 1 mm, corresponding to a reduction level larger than 90%. The oxide scale formed during heat treatment was mechanically removed prior to cold rolling.

3.1. Post-mortem observation of strained Ti-12 wt.% Mo specimens

Dog-bone tensile samples with a calibrated gauge length of 26 mm and width of 6 mm were machined out of the rolled sheets with the tensile direction parallel to the rolling direction. Tensile samples were then reheated at 1173 K for 10 min in air and water quenched to regenerate an equiaxed β + athermal ω (ω_{ath}) microstructure. Again, the oxide layer formed during annealing was mechanically removed using SiC papers and samples were polished with diamond paste to remove the hardened layer. The measured oxygen content prior to mechanical testing was 0.0115 wt.%. The initial grain size was 50 µm.

Interrupted tensile tests were conducted at a strain rate of $5{\cdot}10^{-4}$ s^{-1} on a universal stress rig equipped with a high-resolution extensometer in order to perform TEM observation of deformed microstructure. 3 mm in diameter discs were then machined out from the centre of the tensile samples by electrical discharge machining (EDM), and then mechanically thinned with SiC papers on both sides of the discs to reach a thickness of 200 µm. Twin-jet electropolishing was then conducted with a solution of 4% $HClO_4$ in methanol at −20 °C with an applied voltage of 5 V and a current of 0.05 A. TEM observations were conducted on a FEI-Osiris Field Emission Gun microscope operating at 200 kV.

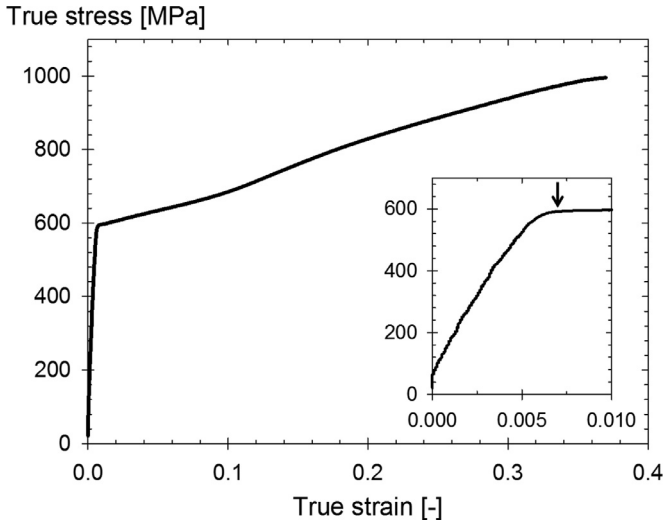

Fig. 2. True stress–true strain curve of the as-quenched Ti-12 wt.% Mo. Inset: magnification of the onset of plasticity with the indication of the strain level at which TEM samples were extracted.

3.2. In-situ observation of {112}<111> mechanical twinning

Fig. 1(a) shows the push-to-pull (PTP) device designed for quantitative in-situ TEM uniaxial tensile tests. A single-tilt PI 95 TEM PicoIndenter (Bruker Inc.) is used to push on the PTP device, inducing a displacement between the two parts located in the white square (see [38–39] for more details). Nanobeams of Ti-12 wt.% Mo were milled from bulk material by focused ion beam (FIB) in a dual beam FIB/SEM instrument. Prior to the FIB preparation, orientation mapping on a wide zone located in the centre of the recrystallised sample had been performed in order to choose particular orientations for the nanobeams (particularly a [110] direction aligned with the electron beam in the TEM). Fig. 1(b) shows the Inverse Pole Figure (IPF) parallel to the rolling direction of the bulk sample with the location where the beam has been extracted by FIB. The sample presents two crystalline orientations with the grain boundary located near the centre of the sample. The stereographic projection given in the inset shows that the thin foil normal is nearly aligned with a ⟨110⟩ zone axis for both grains. Electron-beam assisted Pt deposition was first applied on the surface of the bulk sample

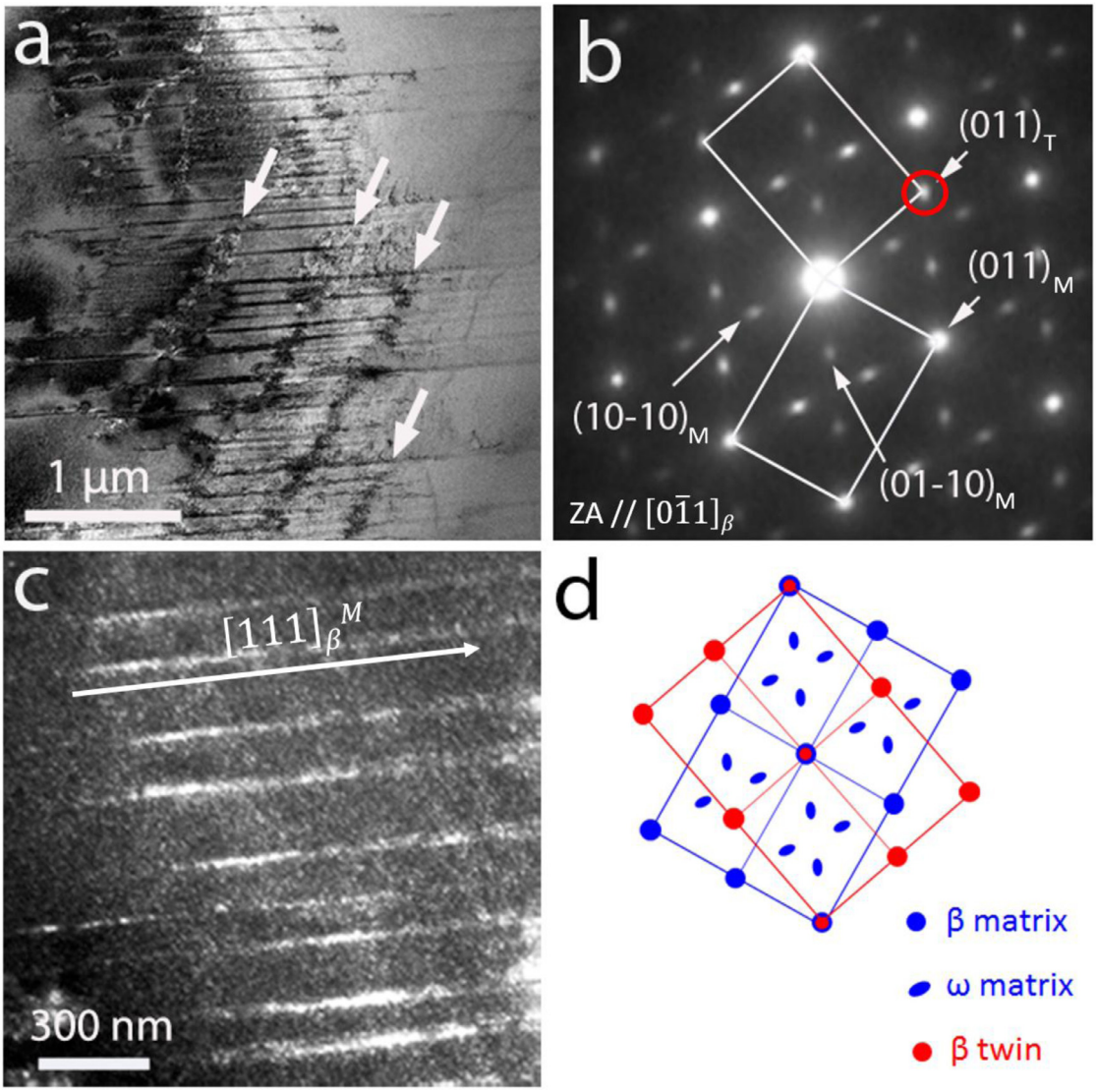

Fig. 3. (a) Bright-Field TEM micrograph of Ti-12 wt.% Mo sample strained to $\varepsilon = 0.007$. The white arrows highlight twinning sources. (b) SAD pattern of the grain shown in (a) taken along a $[0\bar{1}1]_\beta$ zone axis. (c) Dark-Field micrograph of a magnified region from (a) obtained from the (011) spot of the β twin (circled in red in (b)). (d) Key diagram showing the correspondence between the matrix and the twin diffraction patterns along the $[0\bar{1}1]_\beta$ zone axis.

with very low energy electrons (5 kV, 0.8 nA) to avoid damaging the surface, followed by an ion-beam assisted Pt layer deposition (30 kV, 0.23 nA), which prevents the penetration of Ga^+ ions in the top surface of the sample. After the thinning steps, a final cleaning of both sides of the thin lamella was performed using a very low energy ion beam of 1 kV and 95 pA to minimise damage and/or amorphisation. Subsequently, the Ti–Mo thin lamella was cut from both sides using the Ga^+ ion beam to achieve the desired dimensions and transfer it to the PTP device using an Omniprobe micromanipulator on the zone located in the white square of Fig. 1(a), as shown in the magnification in Fig. 1(c). The sample was then attached to the PTP device using electron-beam-deposited Pt (Fig. 1(c)). This layer acts as the jaws of a tensile machine and maintain the sample attached during mechanical testing. The dimensions of the nanobeams are about $4 \times 1 \times 0.2$ µm. The experiment has been performed in load control mode with a stress plateau to observe the plasticity mechanisms. The displacement rate to achieve the first stress plateau was 0.5 nm/s, and the stress was maintained at a level of 2.25 GPa for 240 s before unloading. A second stress plateau at a level of 2.5 GPa was applied to the sample where fracture occurred. The whole experiment has been recorded by a CCD camera with a frequency of 5 Hz.

4. Results

4.1. Post-mortem {112}<111> mechanical twins

True stress-true strain curve of as-quenched bulk Ti-12 wt.% Mo sample is given in Fig. 2. For this study, bulk samples were strained very close to the onset of plasticity ($\varepsilon = 0.007$), corresponding to a macroscopic tensile stress of 600 MPa as highlighted by the inset in Fig. 2. Typical defects resulting from this level of plastic deformation are illustrated in the bright-field (BF) TEM micrograph of Fig. 3(a). A dense stack of parallel straight lamellas can be observed. These defects can be indexed as $\{112\}\langle 111\rangle$ mechanical twins as shown by the selected area diffraction (SAD) pattern taken along a $[\bar{1}10]_\beta$ zone axis in Fig. 3(b). These mechanical twins present a mean thickness of 40 ± 5 nm measured in edge-on orientation, while their mean spacing is 180 ± 50 nm. The dark-field (DF) micrograph of Fig. 3(c), highlighting the twins, corresponds to the $(011)_{\beta T}$ diffraction spot. It is worth noting that it also corresponds to the $(10\bar{1}1)_\omega$ diffraction spot, explaining the observation of homogeneously dispersed nanoscale ω_{ath} precipitates in the matrix in Fig. 3(c). However, the indexation cannot be ensured solely based on the SAD

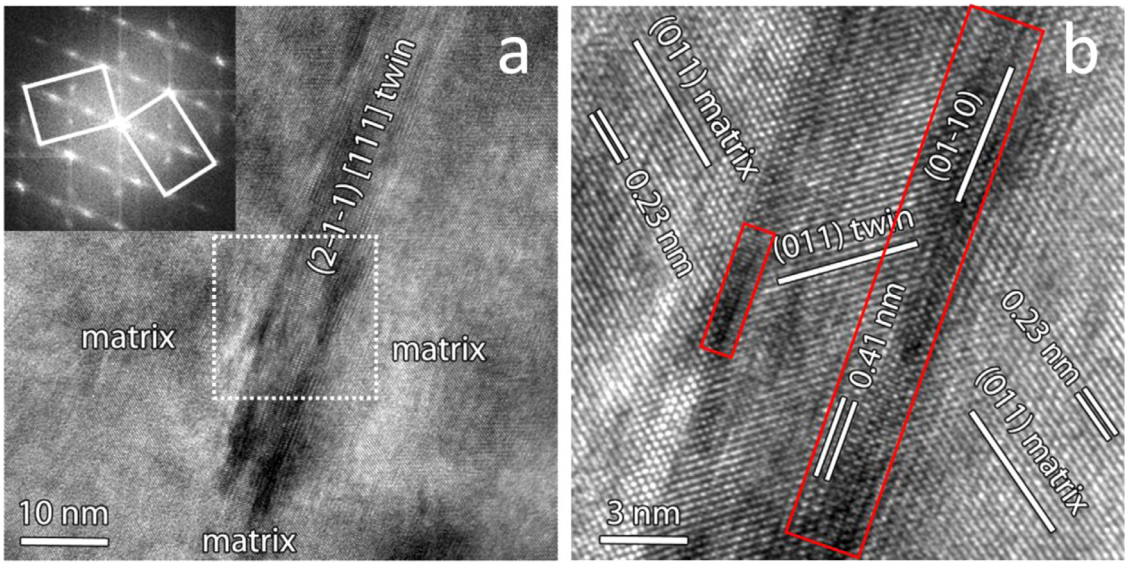

Fig. 4. (a) HR-TEM micrograph of a {112} mechanical twin including a FFT taken from the entire zone shown in (a) as inset and (b) magnification of the white square zone in (a) illustrating the BCC packing within the twin as well as the presence of ω phase at the twin/matrix interface (rectangle dot pattern with 0.41 nm spacing in the red rectangles). (For interpretation of the references to colour in this figure legend, the reader is referred to the web version of this article.)

pattern taken along $[110]_\beta$ since all the diffraction spots from the twins coincide with ω phase spots, as shown in the key diagram of Fig. 3(d).

Fig. 4 exhibits HR-TEM analysis of one of the deformation-induced bands shown in Fig. 3(c). It clearly shows that the band has a BCC stacking with a $\{112\}\langle111\rangle$ twin relationship with the matrix as confirmed by the Fast Fourier Transform (FFT) in the inset. Furthermore, ω phase is observed as a rectangular dot pattern with a spacing of 0.41 nm at the twin/matrix interface with a $(2\bar{1}\bar{1})_\beta \| (01\bar{1}0)_\omega$ lattice coincidence, confirming the limitation of ω reflections to the β matrix as seen in Fig. 3(b).

Fig. 5(a) presents similar features to Fig. 3(a), with a specific emphasis, however, on the defects that seem to be the sources of the identified $\{112\}\langle111\rangle$ twins. The possibility that these defects actually come from shearing of the twins during deformation is discarded since in some cases the number of twins is not the same on both sides of the defects as highlighted by the red rectangles. These defects (indicated by white arrows in Fig. 5(a)) are believed to be jogs initially present in the microstructure. The twins present a thickness of a few tens of nanometres, while their length corresponds to the grain size (tens of micrometres). Fig. 5(b) illustrates the typical interactions between dislocations identified as screw dislocations and the $\{112\}\langle111\rangle$ twins observed in Fig. 5(a). White arrows in Fig. 5(b) depict pinning points of the screw dislocations when encountering the twin bands (indicated by the black arrows). It can also be seen that the dislocations undergo a large amount of cross-slip, which is typical in BCC alloys due to the non-uniqueness of the gliding plane possibilities.

Fig. 5(c) illustrates the twins after tilting the sample far from the edge-on configuration. Discontinuities in the twin boundaries can be observed as emphasized by the white lines. Such discontinuities are important features of the microstructure for further plastic behaviour of the material. Indeed, as shown in Fig. 5(d), the twin boundaries act as very effective dislocation sources. Large numbers of dislocation loops are emitted from the discontinuities in the twin boundaries. Dislocations can also be clearly observed within the twin boundaries as indicated by white arrows in Fig. 5(c). Their origin will be discussed later.

4.2. *Quantitative* in situ *tensile test of nanobeam*

As mentioned in Section 3.2, the tensile FIB-extracted sample presents two crystalline orientations, labelled G1 and G2 for simplicity. Stress–strain curves of the first loading stage of the *in situ* tensile test are given in Fig. 6 for both crystals. The strain values for both grains have been extracted by applying Digital Image Correlation (DIC) on tracked features of the beam. The curve for grain G1 shows a linear relationship between stress and strain on the complete stress range of the test, while grain G2 exhibits a change of slope for a stress level of around 2000 MPa.

Fig. 7(a) shows TEM micrographs of the sample before loading. In this orientation, grain G2 was aligned with $[0\bar{1}1]$ zone axis parallel to the electron beam as shown in the SAD pattern of Fig. 7(c). Grain G1 was slightly tilted from the same zone axis; its SAD pattern along the $[0\bar{1}1]$ zone axis can be seen in the inset of Fig. 7(a). In these conditions, grain G1 has a {111} plane nearly normal to the loading direction (not visible on the SAD pattern). The loading direction of grain G2 is nearly normal to a {112} plane. The theoretical E^{hkl} values for the {111} and {112} families of planes are 110 GPa and 72 GPa, respectively. Fig. 6 shows that the experimental values are very close to the calculated ones (black dotted lines), validating the strain measurement methodology. In this grain, a high density of small dots can be observed in Fig. 7(a). They can be attributed to either FIB-induced damages [40] or to the presence of ω_{ath}. Fig. 7(b) corresponds to the sample after a cycle of loading up to a stress level of 2.25 GPa during 240 s. It can be seen that numerous bands appeared in grain G2, while no specific contrast clearly appeared in grain G1. It should be noted that the sample has been slightly tilted between Fig. 7(a) and (b) to enhance the contrast in G2, which explains the disappearance of numerous aforementioned dots. The dark-field image of Fig. 7(d) corresponds to the $(011)_\beta$ spot. It suggests that the thin bands are in twinning relationship with the matrix. It is worth noting that some variations were detected within the bent contours in grain G1. However, tilting the sample after unloading to orientations close to zone axis or 2-beam conditions did not highlight any lamellas or long dislocations. The irregularities observed at the bent contours are probably due the huge amount of small dots observed in Fig. 7(a) in the same grain. It should also be noted that the bent contours of both grains evolved during the loading plateau, thus suggesting slight rotations of the crystals with respect to the electron beam.

The comparison of Fig. 7(a) and (b) highlights the appearance of numerous nano-twins within grain G2. All these nano-twins formed within a time interval of 0.4 s, corresponding to a strain increment of $5{\cdot}10^{-5}$.

Beside the variations in the bent contours and the formation of nano-twins, Fig. 8 illustrates that a straight line crossing the whole grain G2 appeared within the time interval. This line has been identified as being

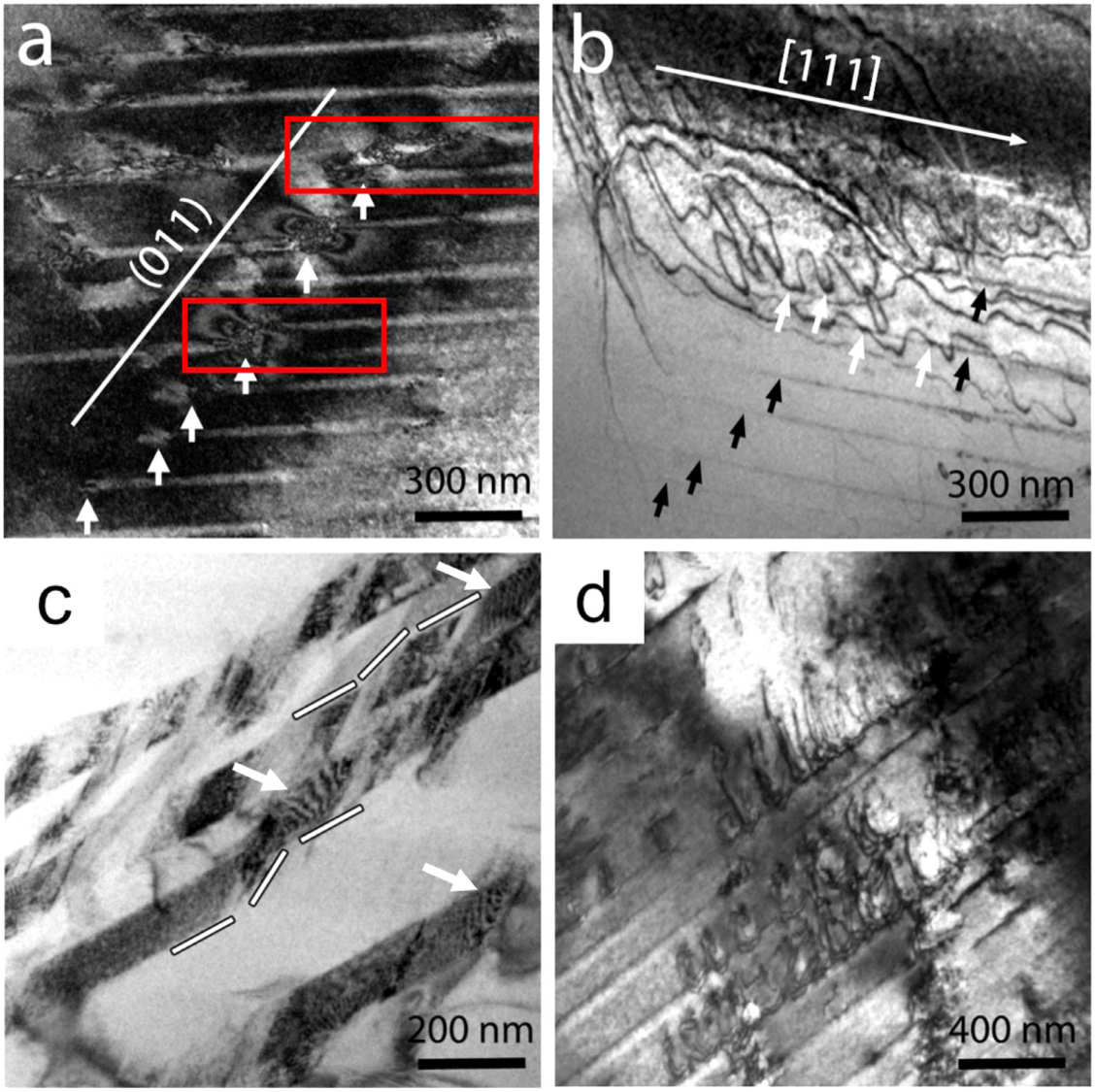

Fig. 5. TEM micrographs illustrating (a) the initially present jogs (white arrows) aligned in a $(011)_{\beta}$ plane and multiple twinning nucleation sites (red rectangles); (b) cross-slip events (white arrows) in screw dislocations due to jog formation resulting from its interactions with twin/matrix interfaces (black arrows); (c) discontinuities (white bars) of the twin boundaries due to super-jogs formation and dislocations within twin boundaries (white arrows); (d) emission of dislocations from the jogged twin/matrix interfaces. (For interpretation of the references to colour in this figure legend, the reader is referred to the web version of this article.)

a perfect $\{321\}\langle 111\rangle$-type screw dislocation by trace analysis on stereographic projection. Indeed, no fringes could be observed while tilting the beam, rejecting the possibility of a stacking fault or an edge-on twin. This dislocation could have nucleated either at the visible grain boundary, or from another defect located in the hidden part of the sample. The measured angle between the nano-twins and the dislocation line is 84°, which corresponds well to the theoretical value of interplanar angle for either the (132) or the $(1\bar{2}\bar{3})$ planes with respect to the $(2\bar{1}1)$ plane (83.74°). Since it was not possible to determine the exact type of dislocation due to the single-tilt sample holder of the push-to-pull device, this dislocation will be called a $\{321\}$-type dislocation in the rest of the text.

The sample has then been reloaded with the same displacement rate up to a second plateau with a higher stress level of 2.5 GPa, where fracture happened quickly within grain G1. Fig. 9 illustrates the evolution of the microstructure during this second loading stage by comparing the same area before (Fig. 9(a)) and during (Fig. 9(b)) loading. Fig. 9(a) illustrates the sample slightly tilted before the second loading cycle to enhance the contrast of the nano-twins. The black arrows highlight some of the twins formed during the first cycle, while the white arrows in Fig. 9(b) show new twins formed just after reaching the second stress plateau. It is worth noting that the former twins do not thicken after reaching a higher stress level.

5. Discussion

In a previous study on the same grade, several plastic deformation mechanisms were identified in the early stages of plasticity, namely mechanical twinning and strain-induced phase transformations [7]. Particularly, deformation products were identified as strain-induced ω phase by conventional SAD. In the present investigation, samples strained to the same level revealed the presence of dense stacks of parallel bands as the one shown in Fig. 3(a). They were identified by high-resolution analysis as being $\{112\}\langle 111\rangle$ twins accompanied by ω phase precipitation on the twin boundaries (Fig. 4). Since all diffraction spots of the twins are superimposed to ω phase spots, high-resolution microscopy is necessary to avoid any confusion. The observation of ω phase precipitation is consistent with the results of Lai et al. [37]. Indeed, this ω phase precipitation would result from the shear process

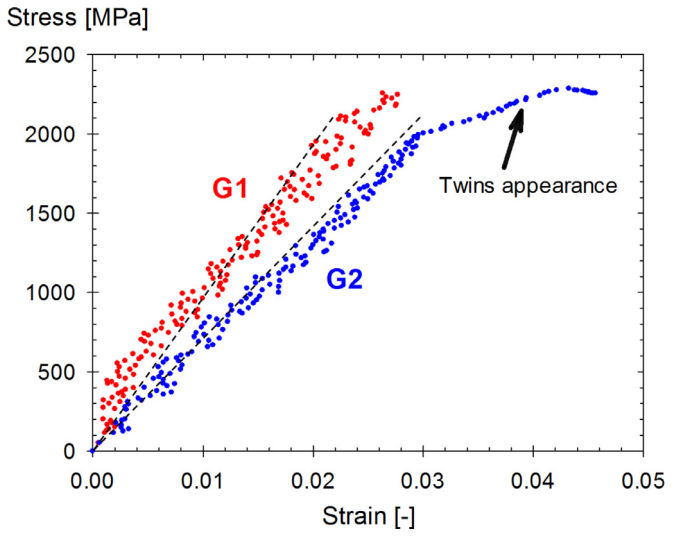

Fig. 6. Stress–strain curves of grains G1 and G2 during the *in situ* TEM first loading cycle. Black dashed lines represent the theoretical moduli of each grain.

involved in $\{112\}_\beta$ twinning that brings enough local elastic energy for triggering this transformation. It is worth noting that a large amount of new interfaces are formed at a strain level as low as $\varepsilon = 0.007$.

The results presented in this work indicate that $\{112\}\langle 111\rangle$ mechanical twinning in the case of as-quenched Ti-12 wt.% Mo alloy requires the existence of numerous thermal jogs within the grains, similarly to previously reported results of Hsiung and Lassila in the case of Ta alloys [28]. It should be mentioned that such defects are too small to be observed in conventional TEM. Indeed, these jogs consist of fragments of dislocations that were not completely annihilated during heat treatments, due to the very low energy associated with such defects. The particular arrangement of the jogs observed in this work, shown by white arrows in Fig. 5(a), can be explained as a result of the scenario schematically represented in Fig. 10. This scenario is similar to the one for pure Nb depicted by Louchet and Kubin [41]. Dislocations move within the grains during cold-working, bringing long straight screw segments due to the velocity difference between edge and screw parts in the BCC structure. Indeed, the strain field associated with the core of the screw segments is spread over several planes containing the Burgers vector direction [20], which increases the frictional forces that need to be overcome compared with non-screw segments. During subsequent heat treatment, the dislocations reorganise themselves, forming a zigzag pattern by climbing to decrease their energy. A helix progressively appears, up to the point where only coaxial prismatic loops remain within the grains. These jogged loops act as dislocation sources once the critical resolved shear stress (CRSS) is reached. The mechanism proposed by Hsiung and Lassila [28] can then be activated.

Jogs are aligned on a (011) plane, which is coherent with the formation mechanism previously presented. Perfect $\frac{a}{2}\langle 111\rangle$ dislocations are emitted from these jogs, which then decompose into three $\frac{a}{6}\langle 111\rangle$ partials that glide on successive {211} planes, inducing the same amount of shear on these planes and resulting in a three-layer micro-twin domain. As pointed out in Section 2.1, Ojha et al. [32] concluded that three-layer twin domains are stable and grow by the incorporation of further dislocations. Since the velocity of twinning screw segments is much smaller than their edge counterparts, the nano-twins present a straight elongated shape, so that they finally present a very limited thickness.

As stated before, a growth mechanism by dislocation incorporation is assumed with further deformation. Numerous twin boundary/dislocation interactions have been observed as illustrated by the white arrows in Fig. 5(b), which seem consistent with the proposed mechanism. The incorporation of screw dislocations has been theoretically discussed in detail by Sleeswyk and Verbraak [1]. It was shown that incorporation could result in growth or shrinkage of the twins, with the creation of jogs at the twin/dislocation intersections. These jogs are normally too small to be observable in conventional TEM microscopy since their height is one or two {112} interplanar distances depending on the Burgers vector of the incoming dislocation. However, the accumulation

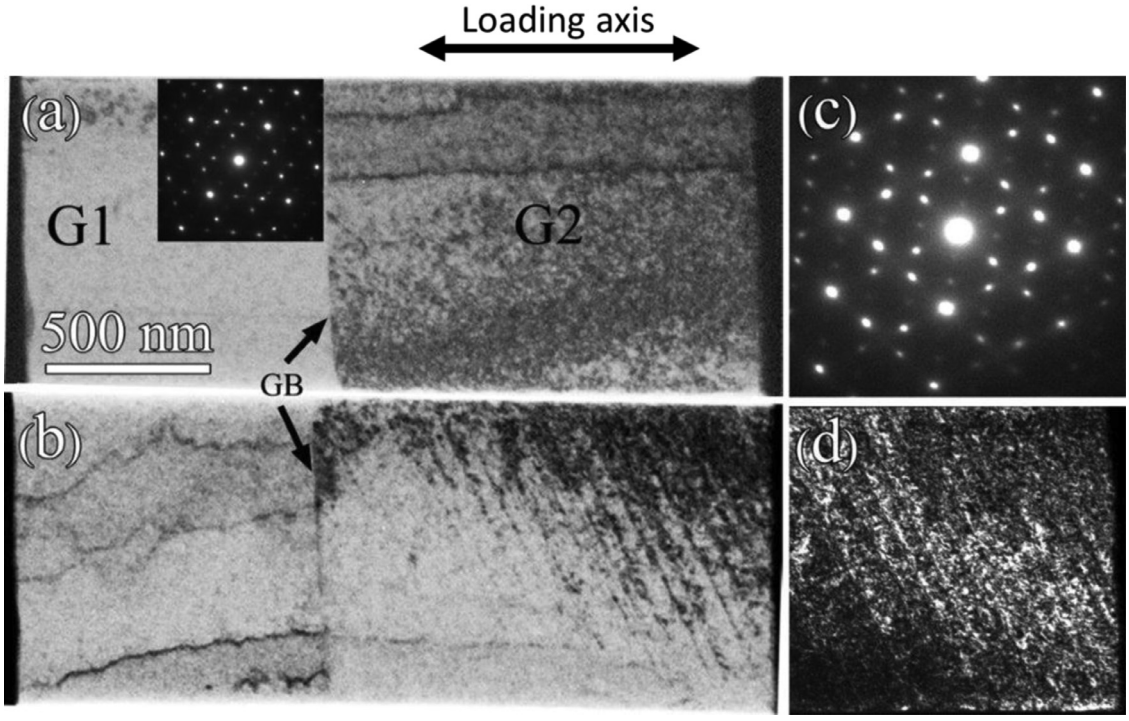

Fig. 7. (a) Bright-Field image of the sample before loading. Inset: SAD pattern of grain G1; (b) bright-field image of the sample after the first loading cycle, showing appearance of numerous bands; (c) SAD pattern of grain G2; (d) dark-field image corresponding to the $(01\bar{1}1)_\omega \| (011)_{\beta'}$ diffraction spot.

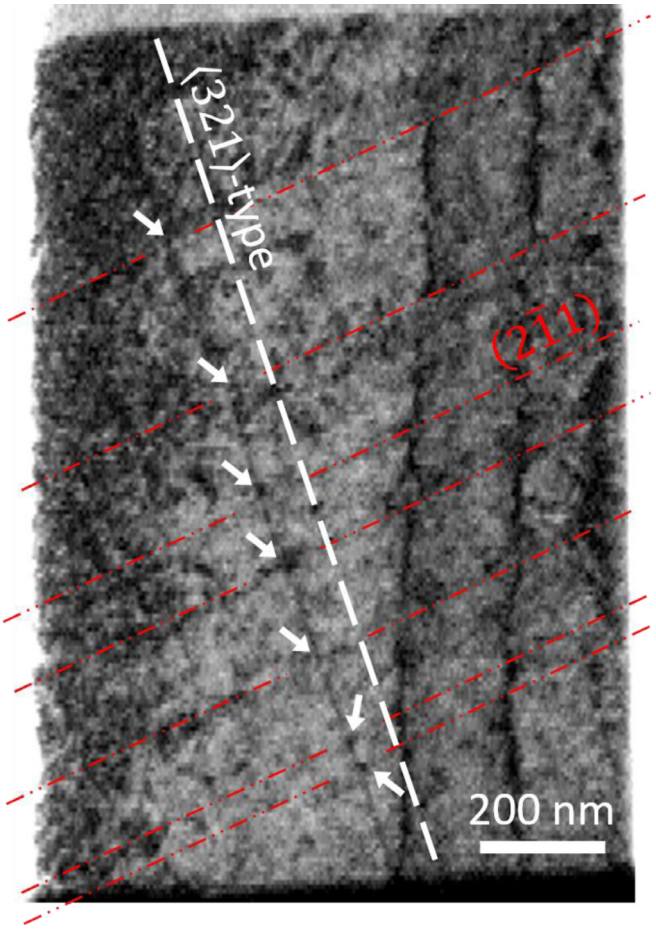

Fig. 8. TEM micrograph of grain G2 rotated 90° just after the appearance of a straight screw dislocation and mechanically induced nano-twins observed in Fig. 7(b). The red dashed lines correspond to some nano-twins while the white arrows highlight the features that could act as nucleation sites for these twins. The thin foil normal is close to [0$\bar{1}$1] zone axis. (For interpretation of the references to colour in this figure legend, the reader is referred to the web version of this article.)

of such incorporation events can progressively bring the formation of "super-jogs". It is postulated that the discontinuities observed in the twin boundaries on Fig. 5(c) are a consequence of these superjogs. Furthermore, the dislocations observed in the tilted twins (Fig. 5(c)) indicate that the growth mechanism involves the incorporation of twinning partials ($\frac{a}{6}\langle 111\rangle$) gliding along the twin boundaries. These growth partial dislocations form due to the dissociation of a perfect dislocation crossing the twin boundaries, as suggested by Sleeswyk and Verbraak [1].

In order to present a high strain-hardening capacity, a large number of dislocation sources must be present in the material, as well as effective obstacles for their motion. It is shown here that the number of dislocation sources rapidly grows within the microstructure. Indeed, the superjogs are very effective dislocation sources as shown in Fig. 5(d). A large number of dislocation loops are emitted from the twin boundaries inside the matrix. The $\{112\}\langle 111\rangle$ twins thus mostly play a role of dislocation sources in the global plasticity of Ti-12 wt.% Mo.

In situ tensile testing of a small-scale sample of Ti-12 wt.% Mo grade exhibited large differences of mechanical behaviour compared to its bulk counterpart. Such differences are generally attributed to the lack of dislocation sources available in the small volumes tested together with the high surface/volume ratio [42]. These effects lead to a large mechanical resistance but very low strain-hardening capacity. Indeed, the density of defects in the volume tested in this work is observed to be very low. The origin of the dislocation highlighted in Fig. 8 has not been identified. It can be assumed that it nucleates from a FIB-induced dislocation loop or from the grain boundary. A better look at this dislocation suggests that the nano-twins nucleate on specific sites on this dislocation (white arrows in Fig. 8), even if the possibility that they nucleate from the surface of the beam cannot be completely discarded. It is worth noting that the enhancement of diffraction contrast of these sites can be explained by the increase of the local strain field due to the interaction of the screw dislocation with some pre-existing ω_{ath} nanoprecipitates or FIB induced nanoclusters, thus leading to cross-slip and the formation of jogs. Such jogs act as preferential nucleation sites for the $\{112\}\langle 111\rangle$ nano-twins, by the partial dislocation mechanism exposed previously and illustrated in Fig. 11 for the particular case of this in-situ tensile test. High resolution analysis could not be performed on the sample after the tensile experiment to validate the proposed mechanism since the sample was highly damaged during the transfer operation to a classical copper grid.

The very high level of stress achieved by the FIB-extracted nanoscale sample is much larger than its bulk counterpart, which is an extrinsic size effect. Moreover, it is coherent with the absence of dislocation activity. However, it is possible that some dislocations appeared in grain G1 without being observed if they were not in the right Bragg conditions, or that newly formed dislocations escape from the sample at free surfaces without being pinned. This last point seems rather unlikely since no strain burst was observed. Furthermore, the surface defects created during FIB preparation as well as the presence of nanoscale ω_{ath} precipitates do not seem to act as dislocation sources, even though the acquisition rate of the recording setup is not fast enough to ensure that the {321}-type screw dislocation observed did not nucleate from such ω_{ath} precipitates. It should also be mentioned that the formation of this

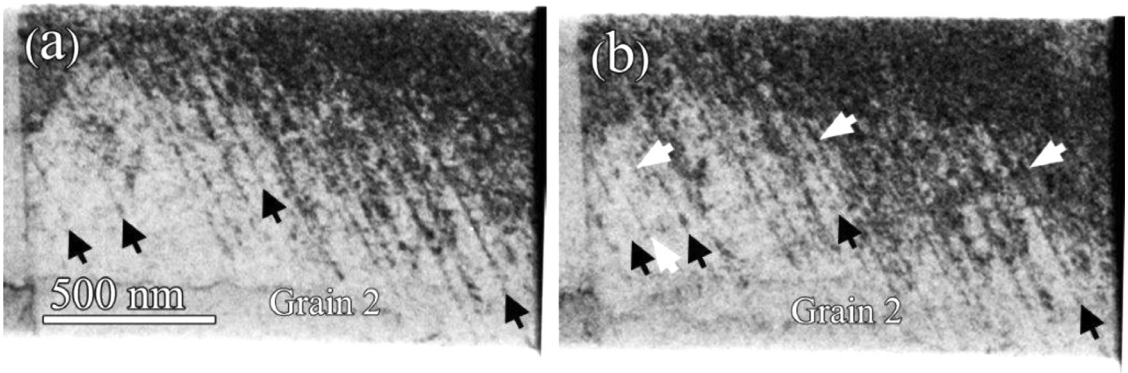

Fig. 9. (a) Bright-Field micrograph of grain G2 of the strained sample after the first loading cycle and (b) during the second stress plateau (2.5 GPa). Black arrows show some twins formed during the first cycle while white arrows highlight new twins formed during the second plateau.

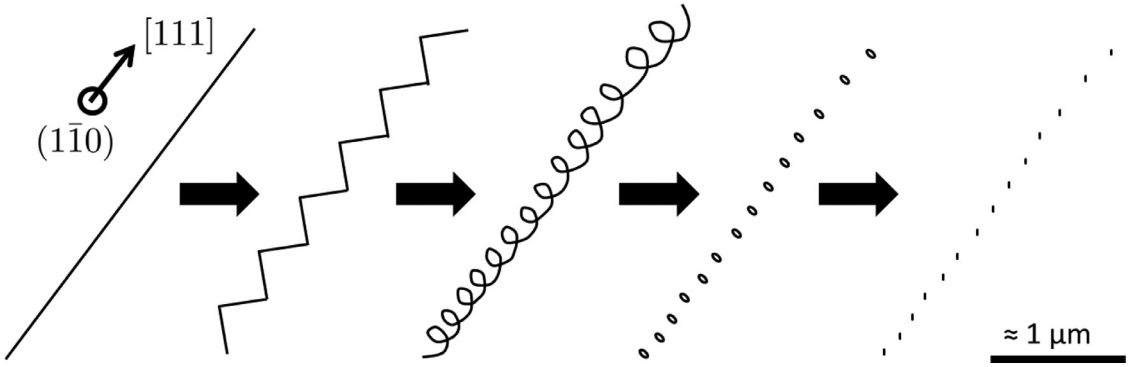

Fig. 10. Schematic representation of the formation mechanism of thermal jogs during heat treatment of BCC lattice.

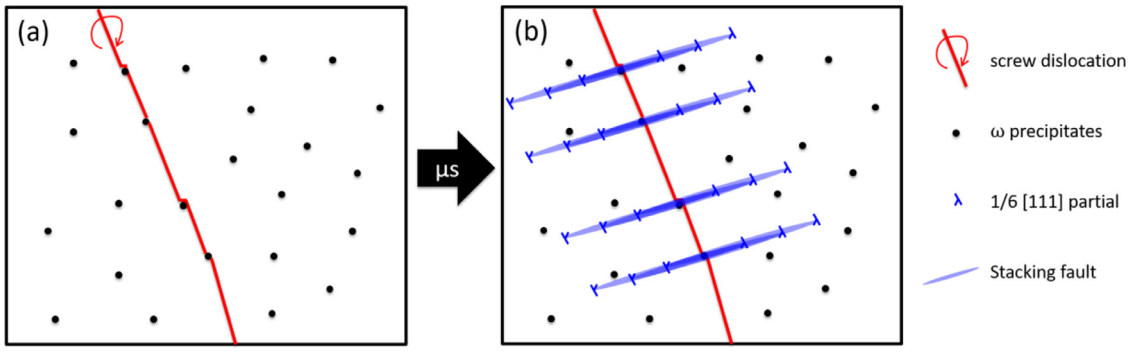

Fig. 11. Schematic representation of the nano-twins formation during the *in situ* tensile test: (a) cross-slipping of the screw dislocation when encountering ω_{ath} precipitates; (b) nucleation of nano-twins on the jogs of the dislocation.

Table 1
Calculated Schmid factors for some slip systems in both grains of the beam shown in Fig. 7.

	Slip system	Schmid factor
G1	[$\bar{1}$11](1$\bar{1}$2)	0.351
	[111](12$\bar{1}$)	0.351
	[$\bar{1}$11]($\bar{1}$10)	0.322
	[$\bar{1}$1$\bar{1}$](132)	0.033
	[1$\bar{1}$1](12$\bar{3}$)	0.033
G2	[11$\bar{1}$](2$\bar{1}$1)	0.386
	[$\bar{1}\bar{1}$1]($\bar{1}$10)	0.334
	[$\bar{1}\bar{1}$1](101)	0.334
	[$\bar{1}$1$\bar{1}$](132)	0.035
	[1$\bar{1}$1](12$\bar{3}$)	0.035

type of dislocation as first active slip system is rather unusual. Indeed, even though these planes are often cited as possible slip planes in the BCC lattice, most of the reported results consider {110}- and {112}-type slip systems [43]. Kaun et al. reported a nearly simultaneous activation of {110} and {321} slip systems during tensile loading of macroscopic BCC single crystals when the loading direction is close to a ⟨110⟩ direction of the crystal [44], which is the case here. Schmid factors of both grains for several BCC slip systems have been calculated, and the obtained values are listed in Table 1. It can be seen that amongst the {110} and {321} slip systems, the highest Schmid factor corresponds to the former type. The activation of a dislocation with such a low Schmid factor (0.035) is quite surprising. However, the very small volume (0.8 µm^3) tested in this experiment does not contain any pre-existing dislocation, so that it has first to nucleate. The nucleation of dislocation does not follow the Schmid factor rule, so it is believed that the Schmid factor is not a correct descriptor in the present situation.

When the load is maintained at a given level, {112} nano-twins with a thickness smaller than 10 nm form quite instantaneously within one of the grains (Fig. 7(b)). It is worth noting that the twins encountering the grain boundary did not cross it, contrarily to {332} twins as reported in previous studies [7,45]. It can be seen in Table 1 that the [11$\bar{1}$](2$\bar{1}$1) slip system of grain G2 presents the highest value of Schmid factor that corresponds to the twin system activated during the experiment. In this case, since fragments of dislocations exists, *i.e.* jogs formed at the intersection between the {321}-type dislocation and ω precipitates, the Schmid factor rule seems to be correctly followed. The activation of a {112} slip plane instead of a {110} one (corresponding to the most dense packing in BCC lattice) has been largely observed in pure BCC refractory metals and interpreted by Seeger [46] as a consequence of the core structure of the screw dislocations based on its theory of kink-pair formation on screw dislocations [47]. Recently, Kamimura et al. proposed a generalised Peierls–Nabarro model and showed that the normalised Peierls stress (τ_p/G) of dislocations is largely dependent on the crystal structure [48]. They showed that the Peierls stresses for BCC transition metals range from $2{\cdot}10^{-3}$ to $8{\cdot}10^{-3}$ G for $\frac{1}{2}\{110\}\langle 111\rangle$ screw dislocations, where G is the shear modulus. This corresponds to stress values of 70–280 MPa in the case of Ti-12 wt.% Mo ($G = 35$ GPa), which seems consistent with the TEM post-mortem observations since numerous twins as well as dislocations have been found in bulk samples loaded up to a macroscopic stress level of 600 MPa (Section 4.1). In this *in situ* experiment, the resolved shear stress corresponding to the highest Schmid factor in grain G2 is equal to $\tau_r = 868$ MPa. This large difference of stress required for the activation of dislocation motion between the bulk and monocrystalline samples can be attributed to the lack (or the small size) of effective dislocation sources in the nanoscale sample. Indeed, the first nanotwins have been observed as soon as one screw dislocation has been formed within the grain. It is interesting to note that the resolved shear stress corresponding to the {321}-type dislocation equals 79 MPa, which lies in the stress range defined by Kamimura [48]. The time resolution of the camera is not sufficient to conclude that the first nanotwins form after the dislocation. However, since some twins have

appeared in a later frame, it can be supposed that the dislocation is mandatory for the formation of twins. The mechanism of mechanical twinning is intimately related to the defect structure of the initial crystal. Once the stress concentration level is reached for generating the first dislocations in the sample, nanotwins are immediately emitted from jogs at the screw segments at a sonic velocity to relax the elastic strain imposed to the sample. Furthermore, the *in situ* TEM observations showed that, in contrast to bulk samples, the twins do not thicken after their nucleation. Again, this indicates that the growth of twins is supported by incorporation of partial dislocations, as suggested by Sleeswyk and Verbraak [1]. This mechanism is hindered in the thin sample by the lack of gliding dislocations. During the second loading plateau at a higher stress level, new twins form again as a relaxation mechanism.

The lack of observation of stable stacking faults suggests that the SFE in the as-quenched Ti-12 wt.% Mo grade is high, consistently with previous calculations of SFE for other BCC materials such as Fe-based alloy [32] and Ti–Nb alloys [49]. A decrease of the SFE with decreasing stability of the β phase of Ti has been confirmed by *ab initio* simulations. However, the lower values of SFE are still quite large compared to FCC alloys (more than 200 mJ/m^2 for the less stable Ti–Nb alloy). Further investigations are necessary to determine experimentally the SFE of the Ti-12 wt.% Mo grade. It is believed that the decomposition of a perfect $\frac{a}{2}\langle 111\rangle$ dislocation in three $\frac{a}{6}\langle 111\rangle$ partials is a metastable state that can exist only when the system is highly stressed. In the absence of twin formation by the mechanism depicted here, these metastable partials will recombine once the stress is removed. Finally, the presence of ω_{ath} precipitates could also be a source of local lowering of the SFE in the alloy, leading to preferential sites for twin nucleation.

6. Conclusion

Both post-mortem observations of deformed samples and quantitative *in situ* tensile testing have been performed to investigate the $\{112\}\langle 111\rangle$ twin nucleation mechanism in the as-quenched Ti-12 wt.% Mo grade. It was shown that this type of mechanical twinning happens at the onset of plasticity, bringing a microstructure presenting such kind of mechanical twins. It seems that these twins essentially play the role of dislocation source for further deformation mechanisms such as $\beta\rightarrow\alpha$" transformation and subsequent $\{332\}\langle 113\rangle$ twinning, since this first plasticity mechanism is substituted by the two latter ones with increasing plastic deformation. Furthermore, a ribbon of ω_{ath} phase appears at the twin boundaries to relax the elastic strain field associated to the creation of the interface.

The present observations are consistent with the nucleation mechanism proposed by Hsiung and Lassila [28], with the initial presence of defects like thermal jogs acting as nucleation sites. Moreover, *in situ* tensile tests on nanoscale samples confirm the need of such nucleation sites for triggering mechanical twinning. The defect-free material does not bring the formation of the partials needed for the formation of twins. In contrast, once a defect such as a screw dislocation appears in the material, the formation of twins is nearly instantaneous in order to relax the elastic strain inside the beam. The initial defect configuration thus plays a major role in the mechanical behaviour of this alloy. Finally, growth of twins arises by partial dislocation incorporation, leading to the formation of superjogs at the twin boundaries, which act as new dislocation sources.

Declaration of interest

None.

Acknowledgments

This work was carried out in the framework of the IAP 7/21 program of the Belgian Science Policy. The Fonds National de Recherche Scientifique FNRS is gratefully acknowledged for the grant no. T.0127.19 and for the mandate of H. Idrissi.

References

[1] A.W. Sleeswyk, C.A. Verbraak, Incorporation of slip dislocations in mechanical twins, Acta Metall. 9 (1961) 917–927.
[2] J. Levasseur, Étude géométrique de l'intersection des macles et de l'interaction macle-glissement dans le fer α, Mater. Sci. Eng. 4 (1969) 343–352.
[3] S. Mahajan, Twin-slip and twin-twin interactions in Mo-35 at.% *re* alloy, Phil. Mag. 23 (1971) 781–794.
[4] M. Marteleur, F. Sun, T. Gloriant, P. Vermaut, P.J. Jacques, F. Prima, On the design of new β-metastable titanium alloys with improved work hardening rate thanks to simultaneous TRIP and TWIP effects, Scr. Mater. 66 (2012) 749–752.
[5] F. Sun, J.Y. Zhang, M. Marteleur, C. Brozek, E.F. Rauch, M. Veron, P. Vermaut, P.J. Jacques, F. Prima, A new titanium alloy with a combination of high strength, high strain hardening and improved ductility, Scr. Mater. 94 (2015) 17–20.
[6] C. Brozek, F. Sun, P. Vermaut, Y. Millet, A. Lenain, D. Embury, P.J. Jacques, F. Prima, A β-titanium alloy with extra high strain-hardening rate: design and mechanical properties, Scr. Mater. 114 (2016) 60–64.
[7] F. Sun, J.Y. Zhang, M. Marteleur, T. Gloriant, P. Vermaut, D. Laillé, P. Castany, C. Curfs, P.J. Jacques, F. Prima, Investigation of early stage deformation mechanisms in a metastable β titanium alloy showing combined twinning-induced plasticity and transformation-induced plasticity effects, Acta Mater. 61 (2013) 6406–6417.
[8] D. Hull, Fracture of Solids, Interscience, 1963, p. 43. New Yorkpage.
[9] A. Gilbert, G.T. Hahn, C.N. Reid, B.A. Wilcox, Twin-induced grain boundary cracking in bcc metals, Acta Metall. 12 (1964) 754–755.
[10] C.N. Reid, A. Gilbert, G.T. Hahn, Twinning and brittle fracture in molybdenum, Trans. Met. Soc. AIME 236 (1966) 1024.
[11] M.J. Marcinkowski, H.A. Lipsitt, The plastic deformation of chromium at low temperatures, Acta Metall. 10 (1962) 95–111.
[12] H. Tobe, H.Y. Kim, T. Inamura, H. Hosoda, S. Miyazaki, Origin of {332} twinning in metastable β-Ti alloys, Acta Mater. 64 (2014) 345–355.
[13] E. Bertrand, P. Castany, I. Peron, T. Gloriant, Twinning system selection in a metastable β-titanium alloy by schmid factor analysis, Scr. Mater. 64 (2011) 1110–1113.
[14] S. Lee, J. Im, Y. Yoo, E. Bitzek, D. Kiener, G. Richter, B. Kim, S.H. Oh, Reversible cyclic deformation mechanism of gold nanowires by twinning–detwinning transition evidenced from *in situ* tem, Nat. Commun. 5 (2014) 3033.
[15] J.W. Christian, S. Mahajan, Deformation twinning, Prog. Mater. Sci. 39 (1995) 1–157.
[16] S. Mahajan, D.F. Williams, Deformation twinning in metals and alloys, Int. Metall. Rev. 18 (1973) 43–61.
[17] M.A. Meyers, O. Vöhringer, V.A. Lubarda, The onset of twinning in metals: a constitutive description, Acta Mater. 49 (2001) 4025–4039.
[18] A.H. Cottrell, B.A. Bilby, A mechanism for the growth of deformation twins in crystals, Phil. Mag. 42 (1951) 573–581.
[19] A.W. Sleeswyk, 1/2< 111>screw dislocations and the nucleation of {112}< 111>twins in the bcc lattice, Phil. Mag. 8 (1963) 1467–1486.
[20] V. Vitek, Theory of the core structures of dislocations in bcc metals, Cryst. Lattice Defects 5 (1974) 1–34.
[21] C. Crussard, Décomposition des dislocations dans le fer et les métaux cubiques centrés, C. R. Hebd. Séanc. Acad. Sci. 252 (1961) 273.
[22] J.B. Cohen, R. Hinton, K. Lay, S. Sass, Partial dislocations on the {110} planes in the bcc lattice, Acta Metall. 10 (1962) 894–895.
[23] V. Vitek, Intrinsic stacking faults in body-centred cubic crystals, Phil. Mag. 18 (1968) 773–786.
[24] J. Demny, Stacking faults in tungsten, Phys. Status Solidi B 22 (1967) K1–K2.
[25] A. Fourdeux, A. Berghezan, Observation by transmission electron microscopy of stacking faults in a body-centered cubic metal: niobium, J. Inst. Met. 89 (1960) 31.
[26] R.L. Segall, Annealing twins and stacking faults in niobium, Acta Metall. 9 (1961) 975–976.
[27] R. Priestner, W.C. Leslie, Nucleation of deformation twins at slip plane intersections in bcc metals, Phil. Mag. 11(1965) 895–916.
[28] L.M. Hsiung, D.H. Lassila, Shock-induced deformation twinning and ω transformation in tantalum and tantalum–tungsten alloys, Acta Mater. 48 (2000) 4851–4865.
[29] J.P. Hirth, J. Lothe, Theory of Dislocations, 2nd, Ed., John Willey & Sons, 1982.
[30] M.L. Kronberg, Atom movements and dislocation structures for plastic slip in single crystals of β-uranium, J. Nucl. Mater. 1 (1959) 85–95.
[31] H. Xing, J. Sun, Mechanical twinning and ω transition by <111>{112} shear in a metastable β titanium alloy, Appl. Phys. Lett. 93 (2008) 031908.
[32] A. Ojha, H. Sehitoglu, L. Patriarca, H.J. Maier, Twin nucleation in fe-based bcc alloys—modeling and experiments, Modell. Simul. Mater. Sci. Eng. 22 (2014) 075010.
[33] R.J. Wasilewski, Mechanism of bcc twinning: shear or shuffle? Metall. Mater. Trans. B 1 (1970) 2641–2643.
[34] B.A. Bilby, A.G. Crocker, The theory of the crystallography of deformation twinning, Proc. R. Soc. London, Ser. A 288 (1965) 240–255.
[35] S.Q. Wu, D.H. Ping, Y. Yamabe-Mitarai, W.L. Xiao, Y. Yang, Q.M. Hu, G.P. Li, R. Yang, {112}< 111>twinning during ω to body- centered cubic transition, Acta Mater. 62 (2014) 122–128.
[36] D. De Fontaine, N.E. Paton, J.-C. Williams, The omega phase transformation in titanium alloys as an example of displacement controlled reactions, Acta Metall. 19 (1971) 1153–1162.

[37] M.J. Lai, C.C. Tasan, J. Zhang, B. Grabowski, L.F. Huang, D. Raabe, Origin of shear induced β to ω transition in Ti–Nb-based alloys, Acta Mater. 92 (2015) 55–63.
[38] H. Idrissi, A. Kobler, B. Amin-Ahmadi, M. Coulombier, M. Galceran, J.-P. Raskin, S. Godet, C. Kübel, T. Pardoen, D. Schryvers, Plasticity mechanisms in ultrafine grained freestanding aluminum thin films revealed by in-situ transmission electron microscopy nanomechanical testing, Appl. Phys. Lett. 104 (2014) 101903.
[39] H. Idrissi, C. Bollinger, F. Boioli, D. Schryvers, P. Cordier, Low-temperature plasticity of olivine revisited with *in situ* TEM nanomechanical testing, Sci. Adv. 2 (2016) e1501671.
[40] H. Idrissi, S. Turner, M. Mitsuhara, B. Wang, S. Hata, M. Coulombier, J.-P. Raskin, T. Pardoen, G. Van Tendeloo, D. Schryvers, Point defect clusters and dislocations in FIB irradiated nanocrystalline aluminum films: an electron tomography and aberration-corrected high-resolution ADF-STEM study, Microsc. Microanal. 17 (2011) 983–990.
[41] F. Louchet, L.P. Kubin, Formation of helical dislocations in pure niobium single crystals under electron irradiation, Radiat. Eff. 26 (1975) 67–69.
[42] A. Pineau, A.A. Benzerga, T. Pardoen, Failure of metals III: fracture and fatigue of nanostructured metallic materials, Acta Mater. 107 (2016) 508–544.
[43] C. Marichal, H. Van Swygenhoven, S. Van Petegem, C. Borca, {110} slip with {112} slip traces in bcc tungsten, Sci. Rep. 3 (2013) 2547.
[44] L. Kaun, A. Luft, J. Richter, D. Schulze, Slip line pattern and active slip systems of tungsten and molybdenum single crystals weakly deformed in tension at room temperature, Phys. Status Solidi B 26 (1968) 485–499.
[45] F. Lin, M. Marteleur, P.J. Jacques, L. Delannay, Transmission of {332}< 113 > twins across grain boundaries in a metastable β-titanium alloy, Int. J. Plast. 105 (2018) 195–210.
[46] A. Seeger, Why anomalous slip in body-centred cubic metals ? Mater. Sci. Eng. A 319 (2001) 254–260.
[47] A. Seeger, The kink-pair-formation theory of the snoek-köster relaxation, Scr. Metall. 16 (1982) 241–247.
[48] Y. Kamimura, K. Edagawa, S. Takeuchi, Experimental evaluation of the peierls stresses in a variety of crystals and their relation to the crystal structure, Acta Mater. 61 (2013) 294–309.
[49] J. Huang, H. Xing, J. Sun, Structural stability and generalized stacking fault energies in β Ti–Nb alloys: relation to dislocation properties, Scr. Mater. 66 (2012) 682–685.